Research Paper

Synthesis of Boron-Aluminum Nitride Thin Film by Chemical Vapour Deposition Using Gas Bubbler

S. Shanmugan and S. D. Mutharasu

**subashanmugan@gmail.com*

Received: April 2018 **Revised: July 2018** **Accepted: September 2018**

Nano Optoelectronics Research Laboratory, School of Physics,Universiti Sains Malaysia (USM), 11800, Minden, Pulau Pinang, Malaysia

DOI: 10.22068/ijmse.16.2.43

Abstract: *Boron (B) doped aluminumnitride (B-AlN) thin films were synthesized on silicon (Si) substrates through chemical vapor deposition (CVD) at 773 °K (500 °C). Tert-butylamine (tBuNH2) solution was used as a nitrogen source and delivered through the gas bubbler. B-AlN thin films were prepared on Si-100 substrates by varied gas mixture ratio of three precursors. The structural properties of the films were investigated from the X-ray diffraction (XRD) data and verified the formation of polycrystalline and mixed phases of hexagonal (100) & (110) oriented AlN and orthogonal (002) & cubic (333) oriented BN. The calculated crystallite size was smaller and hence the dislocation density was higher with lowest total gas mixture ratio (25 sccm). Improved surface properties were detected for the film deposited at lowest total gas mixture ratio by field emission scanning electron microscope (FESEM) and atomic force microscope (AFM) analysis. The film composition showed the existence of a higher concentration of B in the film prepared with lower total gas mixture ratio which was confirmed by energy dispersive X-ray spectroscopy (EDX).*

Keywords: *B-AlN, Thin film synthesis, CVD, Structural parameter, Surface analysis.*

1. INTRODUCTION

Among the group III nitride materials, aluminium nitride (AlN) has been a good candidate in electronic and optoelectronic applications. AlN has several outstanding properties in wide band gap (E_g = 5.9-6.2 eV), good thermal conductivity (280 $Wm^{-1}K^{-1}$), low thermal expansion (≈ 10^{-6} **°C** $^{-1}$), high hardness (1100 Kg/mm^2), a low dielectric constant (8.87) and high acoustic velocity [1-3].

Recently special attention has been paid to improve the properties of AlN through the addition of the third element. There are reports on addition of Cr [4,5] and Si [6,7] as a dopant to enhance the properties of AlN, and some literature proved that addition of Zr [8] and B [9] can improve the thermal conductivity of composite materials. To ensure the producibility of quality AlN thin film, it is necessary to consider the synthesis technique and parameters. AlN thin films can be prepared through various methods such as plasma assisted hot filament chemical vapor deposition [10], hot wall low pressure chemical vapor deposition[11], metal organic chemical vapor deposition method (MOCVD),[12] reactive sputtering [13-15], pulsed laser deposition [16,17], and reactive molecular beam deposition [18]. Among them, CVD has drawn attention due to its advantages such as high deposition rate, no need of ultra-high vacuum , and large area growth capability which is suitable for industrial mass production [19].

There are some traditional CVD techniques such as low pressure CVD (LPCVD) [11], atmospheric pressure CVD (APCVD) [20] , and metal-organic CVD (MOCVD) [12] which are commonly using ammonia gas (NH_3) as nitrogen source from the thermodynamic standpoint. Due to the high thermal stability of NH_3, it requires high substrate temperature typically ≥ 1273 K (1000 °C) to deposit quality AlN thin film. There are reports on the usage of metal-organic precursors such as hexakis (dimethylamido) dialuminum [$Al_2(NMe_2)_6$] [21] and trimethylaluminum [$Al_2(CH_3)_6$] [22] to reduce the substrate temperature, however the precursors are not stable in the presence of oxygen and moisture, which are not

[DOI: 10.22068/ijmse.16.2.43]

easy to handle. In addition, single source precursors such as trimethylaluminium ammonia [($Me_3Al(NH_3)$] adduct [23,24] had been developed to reduce the synthesis temperature and simplify the precursor input during the CVD process, however, the preparation of single-source precursors may involve complex and costly procedures.

In this work, B doped AlN (B-AlN) thin films were deposited on Si(100) substrates by a CVD method with various gas flow rates. Lower deposition temperature 773 K (500 °C) is set for the process todeposit a ceramic film on lower melting point substrates like Al at T < 923 K (650 °C) which is highly suitable for Metal Core Printed Circuit Board (MCPCB) fabrication and also for thermal substrates. In order to deposit nitride film at lower substrate temperature, *tert*-butylamine ($tBuNH_2$) was used as nitrogen source instead of NH_3 due to its suitable vapor pressure (340 Torr at room temperature) [25]. There are reports on the successive deposition of AlN with the use of $tBuNH_2$ at a lower temperature range of 673 – 873 K (400 - 600 °C) [26,27]. Aluminum chloride ($AlCl_3$) was selected as Al source and Boron trichloride (BCl_3) was chosen as B source in the CVD process. The gas bubbler was employed as a liquid precursor delivery system since it is an easier and reliable method to obtain a uniform mixture of gases immediately and successfully used for some other CVD process [28]. So far there is no report on the use of bubbler for $tBuNH_2$ in AlN synthesis using the CVD process. The deposited films were analyzed by using XRD technique for their structural parameters such as crystallite size, dislocation density, residual stress, and strain, etc. The surface morphology was also investigated through FESEM and AFM, respectively.

2. EXPERIMENTAL PROCEDURES

In this experiment, Boron doped AlN thin film was synthesized on Si substrates by CVD process at 773 K (500 °C). The silicon (100) substrates were selected for this study since the thermal expansion coefficient of Si (2.6×10^{-6} °C $^{-1}$) is well matching with that of metal nitrides (10^{-6} °C $^{-1}$) [29]. Before we load the substrate in the quartz tube, the native oxides on the substrates were removed by cleaning using the RCA (Radio Corporation of America) method [30].

A hot wall three zone furnace purchased from MTI Corporation (OTF-1200X-III) was used in this experiment. The cleaned Si substrates were loaded and positioned at the central zone of the CVD tube as shown in the schematic diagram (Fig. 1.). Initially, the air inside the tube was evacuated by a rotary vacuum pump followed by N_2 gas purging for about 5 min. The temperature of each zone were set as shown in Fig. 1. $AlCl_3$ powder (anhydrous sublimed ≥ 98 %, Sigma-Aldrich) was used as Al source in this experiment and positioned at the left zone (Fig.1). $tBuNH_2$ (tert-butylamine) solution (98 %, Aldrich) was used as a nitrogen source and fed into the quartz tube using the gas bubbling setup. For which, the Gas bubbler was employed as a liquid precursor delivery system for the CVD process as it is an easier and reliable method to obtain a uniform mixture of gases immediately [31]. BCl_3 solution (1M solution in hexane, Acros Organics) was used as a boron source and fed into the reaction tube for about 30 minutes by bubbling N_2 carrier gas in BCl_3 solution container (bubbler). The flow

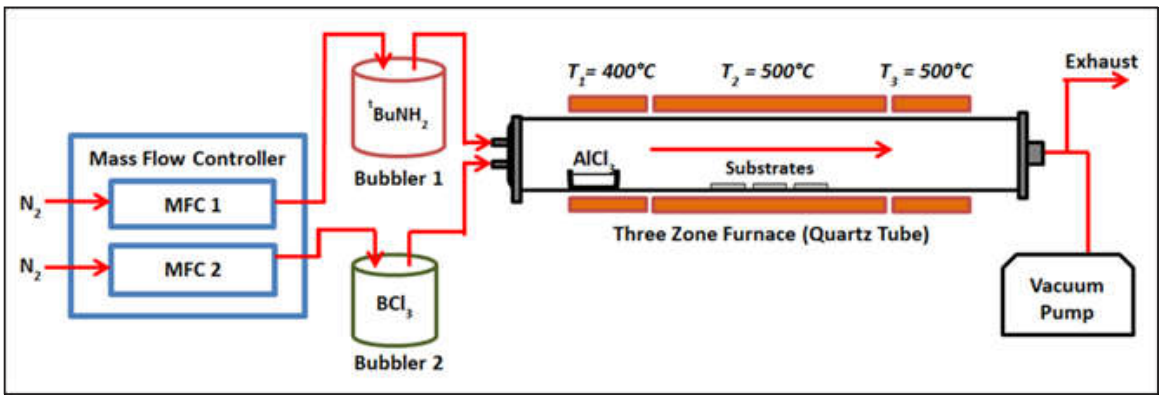

Fig. 1. Schematic diagram of CVD system using the gas bubbler for B-AlN thin film deposition.

[DOI: 10.22068/ijmse.16.2.43]

Table 1. Deposition process parameters of B-AlN thin films by CVD Method.

Process	Precursors	Gas mixture ratio (sccm)	Thickness (nm)
CVD 1	$AlCl_3$ carrier gas (N_2)	10	423
	tert-butylamine	25	
	BCl_3	25	
CVD 2	$AlCl_3$ carrier gas (N_2)	5	440
	tert-butylamine	25	
	BCl_3	25	
CVD 3	$AlCl_3$ carrier gas (N_2)	2.5	498
	tert-butylamine	15	
	BCl_3	15	
CVD 4	$AlCl_3$ carrier gas (N_2)	5	418
	tert-butylamine	10	
	BCl_3	10	

rate of gas for liquid precursor and boron source was controlled by a digital mass flow controller (MFC). The tert-butylamine vapor was released into the tube from left zone and was reacted with $AlCl_3$ at 673 K (400 °C). After that, the mixed vapor was passed through the center zone for one hour where the Si substrates were maintained at 773 K (500 °C) for film deposition at atmospheric pressure. The deposited B-AlN films were subjected to an annealing process at 573 K (300 °C) for 3 hours with a constant flow rate of N_2 gas at 10 sccm in a separate CVD furnace. To get high-quality thin film, the process parameters were optimized by changing four different flow rate of gas as mentioned in Table 1.

In order to evaluate the film quality, the structural properties of B-AlN films such as crystallite size, strain, stress, dislocation density, etc were evaluated by using X-ray diffraction (XRD, X'pert-PRO, Philips, Netherlands) technique with scan range between $2\theta = 25° \& 65°$ and presented for discussion. The surface morphology of the films was also analyzed using field emission scanning electron microscope (FESEM, Nova Nano-SEM 450) and atomic force microscope (AFM, Bruker AXS). The thickness of the prepared thin films was confirmed by the cross-sectional FE-SEM image analysis. In addition, the composition of the films was also investigated by energy dispersive X-ray spectroscopy (EDX) which is attached to the same FESEM equipment. The observed results are presented here for discussion.

3. RESULTS AND DISCUSSION

3.1 XRD Analysis

The XRD spectra of all films are recorded as shown in Fig. 2. It clearly indicates the formation of AlN films with mixed (100) and (110) oriented

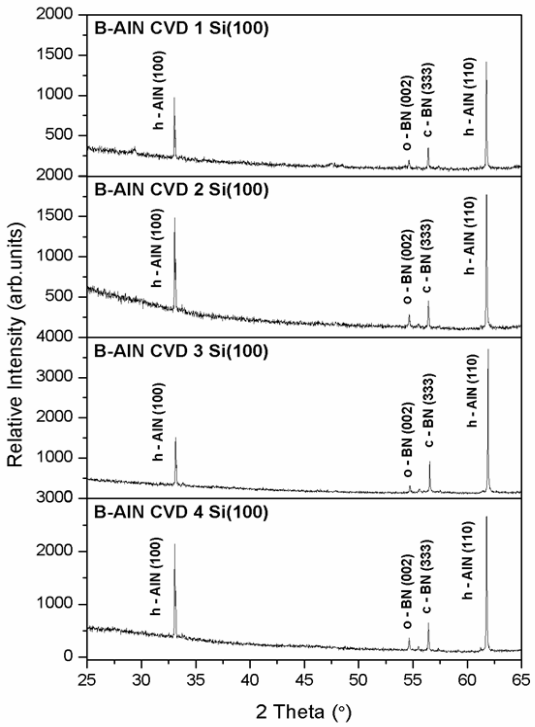

Fig. 2. XRD spectra of B-AlN thin film prepared at various process conditions.

[DOI: 10.22068/ijmse.16.2.43]

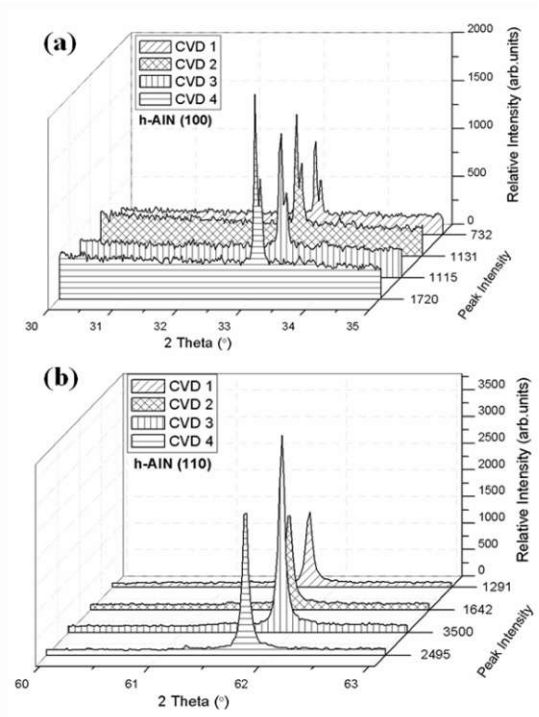

Fig. 3. Variation in XRD peak intensity of (a) (100), and (b) (110) oriented hexagonal AlN.

hexagonal (*h*) phase in all four samples. Besides that, relatively low-intensity peaks related to (002) oriented orthorhombic (*o*) and (333) oriented cubic (*c*) BN phase are also found in the range between (54.5 - 54.7°) and (56.4 - 56.5°). When the carrier gas flow rate (for $AlCl_3$ source) changed from 10 sccm (CVD 1) to 2.5 sccm (CVD 3), an increase in the intensity of (100) oriented AlN peak could be observed and presented in magnified XRD spectra as shown in Fig. 3. Even though the gas flow rate for $AlCl_3$ source increased, high intensity for (100) oriented AlN peak was noticed with CVD process 4 (CVD 4) where the carrier gas flow rates for *tert*-butylamine and BCl_3 were minimized from 25 sccm to 10 sccm when compared with the other three process (CVD 1, CVD 2, and CVD 3) conditions. It is also observed that the total flow rate for all carrier gas is reduced noticeably at CVD 4 process. On considering (110) peak as referred to Fig. 3(b), the intensity gradually increases as the carrier gas flow rates decrease for all precursors. Especially, the high intensity was noticed for (110) peak with CVD 3 process where the carrier gas flow rate for $AlCl_3$ was fixed at 2.5 sccm. It is also noticed that the reduced gas flow rate for *tert*-butylamine and BCl_3 is used and helped to achieve high thickness in this study. Upon decreasing the flow rate of the carrier gas further for *tert*-butylamine and BCl_3 precursors, decreased intensity of (110) peak is noticed where the carrier gas flow rate for $AlCl_3$ is increased from 2.5 sccm to 5 sccm. From the observed results, it is noticed that the low flow rate of $AlCl_3$ (2.5 sccm) is supporting the growth of (110) oriented AlN thin film at a moderate flow rate of the gas for another precursor (CVD 3). In addition to this, the reduced carrier gas flow rates (from 15 sccm to 10 sccm) of *tert*-butylamine and BCl_3 were also supporting this observation. On considering the peak intensity of BN phase, it is noticed that the peak intensity of (002) oriented *o*-BN phase increases from 139 (a.u.) to 217 (a.u.) when the flow rate for BCl_3 reduced from 25 sccm to 10 sccm (CVD 2 to CVD 4 processes). While considering *c*-BN (333) peak, the highest intensity is achieved with the samples prepared using CVD 3 process, and the intensity slightly decreases for the films prepared from CVD 4 process as the flow rate of BCl_3 reduced from 15 sccm (CVD 3 process) to 10 sccm (CVD 4 process).

Overall, the XRD spectra show the polycrystalline behavior of AlN phase along with BN phase with different orientations especially dominated by (100) oriented AlN peak. From the XRD analysis, it is found that the crystalline B-AlN thin film can be synthesized by reducing the total flow rate especially for *tert*-butylamine and BCl_3 precursors. Overall, it is observed that the thin film deposited with CVD 4 process parameters has more crystallinity than other 3 process parameters. According to Song et al. [32], the lack of BN peak in the XRD spectra indicates that the film has either amorphous structure or composed of very small grain sizes. Moreover, the B atoms are diffused into AlN to form (B, Al)N thin film phase during the deposition process where the synthesis was carried out at a high temperature of 773 K (500 **°C**).

3.2 Structural Parameter Analysis

The observed data of all samples from XRD spectra are summarized in Table 2 and compared

[DOI: 10.22068/ijmse.16.2.43]

Table 2. XRD analysis data of B-AlN thin film prepared on Si substrates.

Process	Identity	Observed 2θ (°)	Standard 2θ (°)	FWHM (°)	Observed d-spacing (Å)	Standard d-spacing (Å)
CVD 1	**h-AlN (100)**	**33.02**	**32.97**	**0.056**	**2.710**	**2.715**
	o-BN (002)	54.53	54.76	0.111	1.679	1.675
	c-BN (333)	56.41	56.86	0.078	1.630	1.618
	h-AlN(110)	**61.76**	**59.35**	**0.067**	**1.501**	**1.556**
CVD 2	**h-AlN (100)**	**33.05**	**32.97**	**0.056**	**2.708**	**2.715**
	o-BN (002)	54.65	54.76	0.100	1.678	1.675
	c-BN (333)	56.42	56.86	0.067	1.630	1.618
	h-AlN(110)	**61.77**	**59.35**	**0.067**	**1.501**	**1.556**
CVD 3	**h-AlN (100)**	**33.13**	**32.97**	**0.078**	**2.702**	**2.715**
	o-BN (002)	54.71	54.76	0.100	1.676	1.675
	c-BN (333)	56.55	56.86	0.067	1.626	1.618
	h-AlN(110)	**61.91**	**59.35**	**0.056**	**1.498**	**1.556**
CVD 4	**h-AlN (100)**	**33.06**	**32.97**	**0.056**	**2.707**	**2.715**
	o-BN (002)	54.65	54.76	0.067	1.678	1.675
	c-BN (333)	56.43	56.86	0.056	1.629	1.618
	h-AlN(110)	61.78	59.35	0.056	1.501	1.556

with the standard 2**θ** data (as reference pattern) from XRD analysis software to determine the peak shifting of the observed 2**θ.** The reference pattern no. of (100) and (110) oriented *h*-AlN phases are 01-070-0354 and 00-025-1133, while the reference no. of (002) oriented *o*-BN and (333) oriented *c*-BN are 01-073-0109 and 00-050-1075, respectively. As B source is introduced into the crystal structure, there is a chance to get the peak shift either to the left or right. Peak shifting towards greater angle was detected for both (100) and (110) oriented AlN in all four samples, it is an evidence of the effect of B inclusion in AlN thin film [33]. The peak shifting is because of the lattice defects as a result of B occupying the lattice site of AlN crystal lattice. To understand the structural changes and properties of the prepared thin film, the structural parameters are evaluated from the XRD results and provided for discussion in Table 3. The crystallite size of the synthesized thin film is calculated using the Debye-Scherer formula [34]:

$$D = 0.94\,\lambda / \boldsymbol{\beta}\cos\boldsymbol{\theta} \qquad (1)$$

where **λ** is wavelength (in Angstrom), **β** is the broadening of diffraction peak (in radians), **θ** is the Bragg diffraction angle. The calculated results are as shown in Table 3. For the lattice parameter, there is no significant change in all peaks. This shows that the variation in gas flow ratio has no obvious effect in altering the lattice constant of B-AlN thin films. The internal stress (**σ**) developed in the deposited film is calculated using the relation:

$$\boldsymbol{\sigma} = -\mathbf{E}\,(\mathbf{d}_a - d_0) / (2\,d_0\,Y) \qquad (2)$$

[DOI: 10.22068/ijmse.16.2.43]

Table. 3. Structural parameters of B-AlN thin film prepared on Si substrates.

Process	Identity	Crystallite size (nm)	Lattice parameter (Å)	Internal Stress	Dislocation density (m^{-2})	Strain
CVD 1	**h-AlN (100)**	**147.918**	**2.710**	**0.9365**	**4.57×10^{13}**	**8.24×10^{-4}**
	o-BN (002)	80.489	3.358	4.4088	1.54×10^{14}	9.40×10^{-4}
	c-BN (333)	115.535	8.469	14.3356	7.49×10^{13}	6.35×10^{-4}
	h-AlN(110)	**138.111**	**2.123**	**-19.6667**	**5.24×10^{13}**	**4.89×10^{-4}**
CVD 2	**h-AlN (100)**	**147.927**	**2.708**	**-1.3116**	**4.57×10^{13}**	**8.24×10^{-4}**
	o-BN (002)	89.392	3.356	3.6597	1.25×10^{14}	8.44×10^{-4}
	c-BN (333)	134.512	8.467	13.9039	5.53×10^{13}	5.45×10^{-4}
	h-AlN(110)	**138.122**	**2.122**	**-19.7890**	**5.24×10^{13}**	**4.89×10^{-4}**
CVD 3	**h-AlN (100)**	**106.226**	**2.702**	**-2.5976**	**8.86×10^{13}**	**1.14×10^{-3}**
	o-BN (002)	89.416	3.353	1.6439	1.25×10^{14}	8.43×10^{-4}
	c-BN (333)	134.592	8.450	9.8654	5.52×10^{13}	5.43×10^{-4}
	h-AlN(110)	**165.369**	**2.118**	**-20.8775**	**3.66×10^{13}**	**4.07×10^{-4}**
CVD 4	**h-AlN (100)**	**147.931**	**2.707**	**-1.4924**	**4.57×10^{13}**	**8.23×10^{-4}**
	o-BN (002)	133.418	3.356	3.7768	5.62×10^{13}	5.66×10^{-4}
	c-BN (333)	160.937	8.467	13.7959	3.86×10^{13}	4.55×10^{-4}
	h-AlN(110)	165.255	2.122	-19.8112	3.66×10^{13}	4.08×10^{-4}

Where d_0 and d_a are the d spacing of bulk and thin film forms respectively [35]. E and Y are Young's modulus (AlN - 308 GPa; BN - 748 GPa) [36,37] and Poisson's ratios of (AlN - 0.29; BN – 0.19) [38,39], respectively.The nature of applied stress during the growth of crystal could be identified by the sign of the observed stress value. If the stress value is positive, it represents the compressive stress, and if it is negative, the tensile stress is applied during the growth process.

From Table 3, it is noticed that the tensile stress is applied during the growth of (110) oriented AlN phase for all samples and it is because of decreased carrier gas flow rate of $AlCl_3$ during the synthesis process. It is also noticed from Table 3 that the compressive stress is also applied during the growth of (100) oriented AlN thin film phase at CVD1 condition. Overall, tensile stress is dominated with the AlN phase for all CVD processing conditions and observed from all samples. But there is not much difference in tensile stress as the carrier gas flow rate changes for all precursors. From this observation, it is concluded that the reduced stress (tensile stress) is possible with higher film thickness. In addition to these, there are few BN peaks being observed thet influencethe internal stress of the film. For (333) oriented *c*-BN phase, the applied compressive stress diminishes as carrier gas flow rate of $AlCl_3$ reduces. In (002) oriented *o*-BN phase, it could be observed that there is a conversion from compressive to tensile stress as the carrier gas flow rate of $AlCl_3$ decreases. According to ref. [40-42], residual stresses play a significant role in the reliability of thin films and cause film buckling or cracking under the existence of large residual stresses and even interface delamination. Overall, it is observed form the residual stress analysis that

[DOI: 10.22068/ijmse.16.2.43]

the film treated with CVD 3 process conditions will have good film quality with higher thickness. Moreover, it is achieved with optimized BCl_3 flow rate (15 sccm) during the process.

In addition to this, dislocation density (**δ**), defined as the length of dislocation lines per unit volume of crystal, was evaluated from the following relation [43]:

$$\delta = 1 / D^2 \quad (3)$$

The strain (**ε**) is calculated from formula using XRD results:

$$\varepsilon = \beta \cot \theta / 4 \quad (4)$$

From Table 3, it shows that the dislocation density observed from (100) oriented AlN phase displays high value for the film deposited using CVD 3 than all other process conditions used in this study. It seems that the crystalline defects are dominated in this phase. On considering (110) phase, the dislocation density decreases as the carrier gas flow rate for $AlCl_3$ decreases and also for other precursors. It is due to the release of stress during the growth at this process condition and hence higher thickness achieved in this process condition [44]. As a result, a highly intensive peak of (110) orientation is observed with CVD 3 process conditions. The line widths of the Bragg peaks provide information on the average grain size and defects of the crystal lattice originating from microstrain. As observed for the dislocation density, the strain developed during the growth of (100) orientated film increases and shows high value for the film processed at CVD 3. The strain in the film defines the ordering of the atoms in the crystal lattice and the concentrations of stacking faults and point defects [45]. For our study, the increased strain reveals the disordering of atoms, stacking faults and point defects in the processed thin film samples. Table 3 also shows the variation of strain in the BN crystal lattice and it decreases as the carrier gas flow rate of all precursor decreases for both orthogonal (002) and cubic (333) phases. It exhibits the formation of BN in the AlN structure with fewer defects.

3.3 FESEM and EDS Analysis

To understand the influence of gas flow rate on the surface morphology of B-AlN thin films, the film surface images were captured by the FE-SEM as shown in Fig. 4 and analyzed the surface

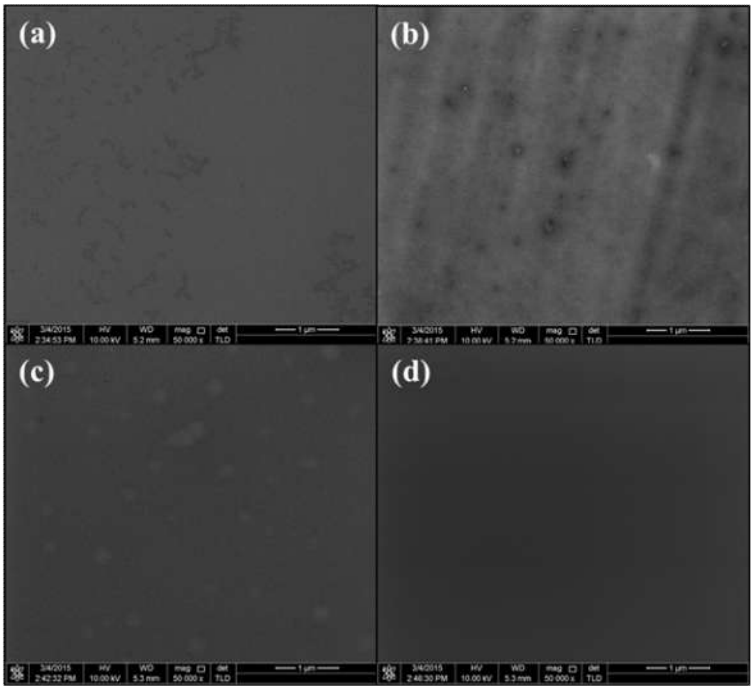

Fig. 4. FESEM images of B-AlN thin film surface prepared using (a) CVD 1, (b) CVD 2, (c) CVD 3, and (d) CVD 4 conditions.

[DOI: 10.22068/ijmse.16.2.43]

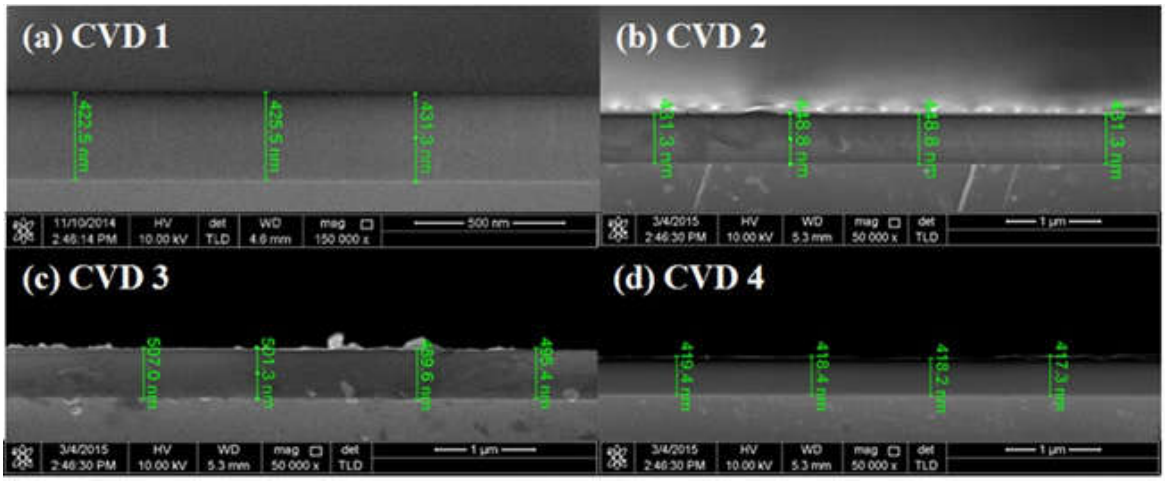

Fig. 5. FESEM cross-section images of the thin film samples prepared at various process conditions.

quality. From the SEM images, the thin film deposited with the highest total gas flow rate (CVD 1) (Fig.5a) has some surface defects. For CVD 2 (Fig. 4b), the surface damages such as pores and flaws can be clearly seen on the film surface as the flow rate of carrier gas for $AlCl_3$ reduced to 50% from that of CVD1. Some small clusters can be observed on the surface of film using CVD 3 condition as shown in Fig. 4c. Good surface morphology is noticed with thin film prepared with the lowest total gas flow (CVD4), which has a smooth surface without any cluster or particle as presented in Fig. 4d. Overall, the lower total gas flow rate released, the smoother the surface of the film can be obtained. Since we changed the gas ratio, it is expected to change the elemental composition of the prepared thin film and should be addressed. To evaluate this, EDS analysis was performed for all samples and observed the elemental compositions as mentioned in Table 4.

During the analysis, the scan area was fixed approximately 25 μm^2. A small decrease in the percentage of Al can be noticed as the total gas flow rate decrease from 60 to 25 sccm (CVD 1 to 4) where the carrier gas flow rate of $AlCl_3$ decreases from 10 sccm to 2.5 sccm. An interesting result could be observed that the nitrogen content increases as the tBuNH$_2$ gas flow rate decreases from 25 to 10 sccm . The percentage of Boron content is relatively low in all samples and can be explained by the diffusion behavior of B atoms into the crystal structure of the film. It is observed that the higher B content is possible only with CVD 3 process conditions while noticing the higher thickness in the same CVD 3. The lower percentage of B content may also be due to insufficient temperature for B source in the gas mixture to react and diffuse into the film structure during the deposition process [32]. It is suggested to increase the B addition by varying the synthesis parameters such as deposition temperature in future work.

To measure the thickness of all samples, the CVD samples were undergone to cross-sectional analysis using FESEM and marked on the images as shown in Fig. 5 and observed average thickness are also given in Table 1. The thickness of all B-AlN thin films were verified by measuring at different points in the cross-sectional image and took the average as given in Table 1. It can be observed that the average thickness of all deposited films with different parameters is in the range of 400 – 500 nm and shows a small deviation between each sample. The film thickness of CVD 1 and CVD 4 samples shows nearly closer value even though there is a huge difference in total gas flow rate. This reveals that a small change in total gas flow rate does not have a significant effect on the thickness. From all samples, B-AlN thin film prepared with CVD 3 process parameter shows higher thickness than other samples. We believe that the deposition rate may increase by changing other parameters like substrate temperature or the total pressure of the tube during the synthesis process.

[DOI: 10.22068/ijmse.16.2.43]

3.4 AFM Analysis

The 3D surface topography of B-AlN thin films is captured by AFM using tapping mode at scan range of 10 **µm** x 10 **µm** and the recorded images are presented in Fig. 6. Based on the process parameters, noticeable changes in the surface morphology could be recorded for all samples which are clearly exhibited in Fig. 6. As we observed from the SEM analysis, smooth surface with low surface roughness and small particle size are expected with the samples prepared using low flow rate of B and N source precursor (CVD 4).

In order to evaluate the surface properties in detail, the surface roughness and particle size were measured from 3D images using image software and their values are summarized in Table 4. The thin film deposited with the highest total gas flow rate (CVD 1) or highest carrier gas flow rate of $AlCl_3$ shows high surface roughness of 0.78 nm. It is noticed that as the surface roughness decreases as the total gas flow rate decreases. The thin film deposited with the lowest total gas flow rate (CVD 4) achieves the lowest roughness. Using the software analysis, the particle size of all thin film are measured from AFM images and also summarized in Table 4. As a consequence, the film

Table 4. Atomic weight percentage, surface roughness and particle size of B-AlN

Process	Weight (wt%)			Roughness (nm)	Particle Size (nm)
	B	Al	N		
CVD 1	0.40	90.18	9.42	0.780	303.050
CVD 2	0.73	89.97	9.30	0.746	320.062
CVD 3	1.70	88.00	10.30	0.759	521.530
CVD 4	1.11	88.48	10.41	0.535	224.751

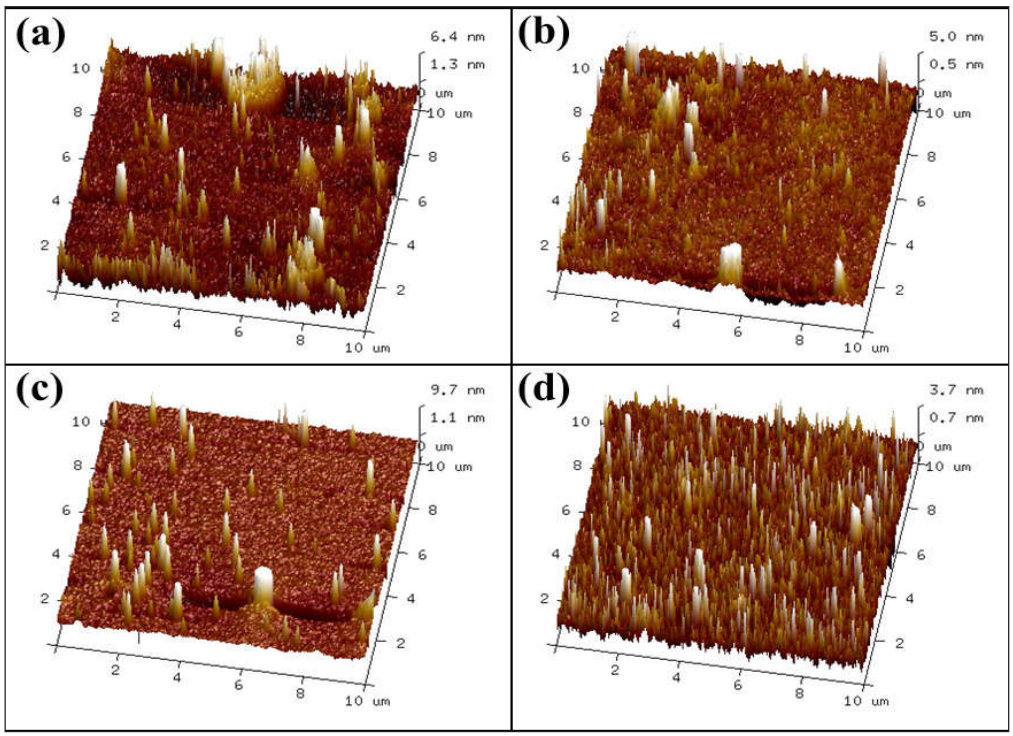

Fig. 6. The AFM (3D) images of B-AlN thin film prepared using (a) CVD 1, (b) CVD 2, (c) CVD 3, and (d) CVD 4 process conditions.

[DOI: 10.22068/ijmse.16.2.43]

prepared with CVD 3 process conditions has bigger particles than the particle size of other films. It is observed from Table 4 that the low value in particle size is also noticed with the film prepared at a reduced flow rate with all carrier gases.

4. CONCLUSION

In this work, B-AlN was successfully deposited on Si(100) substrates using CVD method at a low temperature of 773 K (500 °C) with tBuNH$_2$ as an alternative nitrogen source using the gas bubbler. The XRD analysis result revealed the formation of mixed (100) and (110) oriented hexagonal phase of AlN with polycrystalline BN (cubic and orthogonal) phases. The observed peak shifting suggested the existence of B in the crystal structure of AlN. The structural analysis revealed defects in the crystalline quality as a result of changing the gas mixture ratio. The higher atomic weight percentage of B was observed in the films deposited with lower total gas mixture ratio. Using FESEM and AFM, the improved surface properties were also noticed from the film grown with lower total gas mixture ratio in CVD 4 process condition as the XRD peak intensity of (100) oriented AlN phase was the highest among all four deposition parameters.

ACKNOWLEDGMENT

The authors would like to thank Collaborative Research in Engineering, Science and Technology (CREST) who financially supporting the project with grant (304/PFIZIK/650601/C121). Authors want to extend their gratitude for Master students who collects the data and information for this work.

REFERENCES

1. Motamedi, P. and Cadien, K., "Structural and optical characterization of low-temperature ALD crystalline AlN," J. Cryst. Growth., 2015, 421, 45-52 .
2. Goerke, S., Ziegler, M., Ihring, A., Dellith, J., Undisz, A., Diegel, M., Anders, S., Huebner, U., Rettenmayr, M. and Meyer, H. G., "Atomic Layer Deposition of AlN for Thin Membranes Using Trimethylaluminum and H2/N2 Plasma," Appl. Surf. Sci. 2015, 338, 35-41.
3. Park, M. H., Kim and S. H., "Thermal conductivity of AlN thin films deposited by RF magnetron sputtering," Mater. Sci. Semicon. Proc., 2012, 15, 6-10
4. Felmetsger, V. V., Mikhov, M. K., Reactive magnetron sputtering of piezoelectric Cr-doped A1N thin films, In 2011 IEEE International Ultrasonics Symposium, 2011, 835-839.
5. Tatemizo, N , Imada, S , Miura, Y , Yamane, H and Tanaka, K, "Electronic structure of AlCrN films investigated using various photoelectron spectroscopies and ab initio calculations," J. Phys.: Condens. Matter, 2017, 29, 085502 .
6. Simeonov, S., Bakalova, S., Szekeres, A., Minkov, I., Socol, G., Ristoscu, C. and Mihailescu, I., "Electrical characterization of Si doped AlN films synthesized by pulsed laser deposition," Eur. Phys. J. Appl. Phys. 2015, 70, 10102.
7. Thapa, S. B., "Institute of Optoelectronics, Ulm University, Annual report 2007, 2007, 85.
8. Chu, K., Jia, C., Guo, H. and Li, W., "On the thermal conductivity of Cu–Zr/diamond composites," Materials & Design, 2013, 45, 36-42.
9. He J., Zhang H., Zhang Y., Zhao Y., Wang X., Effect of boron addition on interface microstructure and thermal conductivity of Cu/diamond composites produced by high temperature–high pressure method, Physica Status Solidi (a), 2014, 211, 587-594.
10. Alizadeh, M., Mehdipour, H., Ganesh, V., Ameera, A. N., Goh, B. T., Shuhaimi, A. and Rahman, S. A., "Plasma-assisted hot filament chemical vapor deposition of AlN thin films on ZnO buffer layer: toward highly c-axis-oriented, uniform, insulative films," Appl. Phys. A, 2014, 117, 2217-2224.
11. Heinselman K.N., Brown R. J.. Shealy J. R., "Hot-wall low pressure chemical vapor deposition growth and characterization of AlN thin films, J. Crystal." Growth, 2017, 475, 286-290.
12. Radtke, G., Couillard, M., Botton, G. A., Zhu, D. and Humphreys, C. J., "Structure and chemistry of the Si(111)/AlN interface, Appl. Phys. Lett." 2012, 100, 011910.
13. Moreira, M. A., Doi, I., Souza, J. F., and Diniz, J. A., "Electrical characterization and morphological properties of AlN films prepared by dc reactive magnetron sputtering, Microelec." Engg., 2011, 88, 802-806.
14. Cho, S., "Effect of nitrogen flow ratio on the structural and optical properties of aluminum nitride thin films, J. Crystal Growth," 2011, 326, 179-182.
15. Meng, X., Yang, C., Chen, Q., Gao, Y., Yang, J., "Preparation of highly c-axis oriented AlN films on Si substrate with ZnO buffer layer by the DC magnetron sputtering, Mater." Lett. 2013, 90, 49-52.
16. Biju, Z., Wen, H., "Cubic AlN thin film formation

[DOI: 10.22068/ijmse.16.2.43]

on quartz substrate by pulse laser deposition,"J. Semicond., 2016, 37, 063003.
17. Wang, W., Yang, W., Liu, Z., Wang, H., Wen, L., and Li, G., "Interfacial reaction control and its mechanism of AlN epitaxial films grown on Si(111) substrates by pulsed laser deposition," Sci Rep. 2015, 5, 11480.
18. Schupp, T., Lischka, K., and As, D. J., "MBE growth of atomically smooth non-polar cubic AlN, J. Crystal Growth," 2010, 312, 1500-1504.
19. Barron, A. R., "Open Stax CNX," Jul 14, 2009.
20. Egashira, Y., Kim, H. J., Komiyama, H., "Cluster Size Determination in the Chemical Vapor Deposition of Aluminum Nitride, J. of American Ceram." Soc. 1994, 77, 2009-2016.
21. Gordon, R. and Hong, D., "US patent, Selective sealing of porous dielectric materials," US 20080032064 A1, 2008.
22. 6RZ 2 2011 Trimethylaluminum Wikipedia Information February 12 2011 white smoke.pdf, 2011.
23. Inagakiz, Y. and Kozawa, T., "Chemical Reaction Pathways for MOVPE Growth of Aluminum Nitride," ECS J. Solid State Sci. Technol. 2016, 5, 73-75.
24. Georgieva, K. A., Ciechonski, R. R., Forsberg, U., Lundskog, A. and Janzén, E., "Hot-Wall MOCVD for Highly Efficient and Uniform Growth of AlN, Cry." Growth and Design, 2008, 9, 880-884.
25. Shanmugan, S. and Mutharasu, D., "Testing and Analysis of Boron-Doped Aluminum Nitride Thin-Film-Coated Al as Thermal Substrates in PCB Fabrication for LED Application," IEEE Trans. on Elect. Devic., 2016, 63, 4839-4844.
26. Miikkulainen, V., Suvanto, M. and Pakkanen, T., "Atomic Layer Deposition of Molybdenum Nitride from Bis(tert-butylimido)-bis(dimethylamido) molybdenum and Ammonia onto Several Types of Substrate Materials with Equal Growth per Cycle," Chem. Mater. 2007, 19, 263-269.
27. Miikkulainen, V., Suvanto M. and Pakkanen, T., "Bis(tert-butylimido)-bis(dialkylamido) Complexes of Molybdenum as Atomic Layer Deposition (ALD) Precursors for Molybdenum Nitride: the Effect of the Alkyl Group," Chem. Vap. Deposition, 2008, 14, 71-77.
28. Sapsanis, C., Omran, H., Chernikova, V., Shekhah, O., Belmabkhout, Y., Buttner, U., Eddaoudi, M. and Salama, K. N., "Insights on Capacitive Interdigitated Electrodes Coated with MOF Thin Films: Humidity and VOCs Sensing as a Case Study," Sensors 2015, 15, 18153.
29. Dobkin, D. and Zuraw, M. K., "Springer Science & Business Media," 2013.
30. Jin, S., "Advances in thermal management materials for electronic applications, JOM Journal of the Minerals," Metals and Materials Society, 1998, 50, 46-46.
31. Zang, Y., Li, L. B., Chu, Q., Han, Y., Pu, H., Feng, X. and Jin, H., "Growth of graphene/Ge/Si heterostructure on Si(0 0 1) substrate," Materials Letters, 2017, 205, 162-164.
32. Mah, J. W., Shanmugan, S., Ong, Z. Y., Mutharasu, D. D. and Azmi, A. N., "Thermal substrates for efficient heat dissipation in LED packaging application." In Electronics Manufacturing Technology (IEMT) & 18th Electronics Materials and Packaging (EMAP) Conference, 2016 IEEE 37th International. IEEE.
33. Song, J. H., Huang, J. L. and Lu, J. C. "Sung, Investigation of wurtzite (B,Al) N films prepared on polycrystalline diamond," Thin Solid Films, 2007, 516, 223-227.
34. Salaken, S. M., Farzana, E. and Podder, J., "Effect of Fe-doping on the structural and optical properties of ZnO thin films prepared by spray pyrolysis," Journal of Semiconductors, 2013, 34, 073003.
35. Prepelita, P., Medianu, R., Sbarcea, B., Garoi, F. and Filipescu, M. "The influence of using different substrates on the structural and optical characteristics of ZnO thin filmsApplied," surface science, 2010, 256,1807-1811.
36. Gerlich, D., Dole, S. L., and Slack, G. A., "Elastic properties of Aluminum Nitrdie," Journal of Physics and Chemistry of Solids 1986, 47, 437-441.
37. Levinstein, M., Rumyantsev, S. and Shur, M., "Handbook Series on Semiconductor Parameters," World Scientific, London, 1999, 1, 2.
38. Thokala, R., and Chaudhuri, J., "Calculated elastic constants of wide band gap semiconductor thin films with a hexagonal crystal structure for stress problems," Thin Solid Films, 1995,266, 189-191.
39. Stokes, A. R., Wilson, A. J. C., "The diffraction of X rays by distorted crystal aggregates" , I, Proceedings of the Physical Society, 1944, 56, 174 - 181.
40. Freund, L. B. and Suresh, S., "Thin film materials: stress, defect formation and surface evolution. "Cambridge University Press, 2004.
41. Moon, M. W., Jensen, H. M., Hutchinson, J. W., Oh, K. H. and Evans A. G., "The characterization of telephone cord buckling of compressed thin films on substrates," J. of Mech. and Phy. of Solids, 2002, 50, 2355.
42. Lee, A., Clemens, B. M. and Nix, W. D, "Stress induced delamination methods for the study of adhesion of Pt thin films to Si," Acta Materi., 2004, 52, 2081-2093.
43. Williamson, G. K. and Smallman, R. E., "Dislocation densities in some annealed and cold-

[DOI: 10.22068/ijmse.16.2.43]

worked metals from measurements on the X-ray debye-scherrer spectrum," Philos. Maga., 1956, 1, 34-46.
44. Mahalingam, T., John, V. S. and Hsu, L. S., "Microstructural analysis of electrodeposited zinc oxide thin films, Journal of New Materials for Electrochemical Systems", 2007, 10, 9-14.
45. Rupp, J. L., Infortuna, A. and Gauckler, L. J., "Microstrain and self-limited grain growth in nanocrystalline ceria ceramics," Acta Materialia, 2006, 54, 1721-1730.

[DOI: 10.22068/ijmse.16.2.43]